HHS Public Access

Author manuscript

Glia. Author manuscript; available in PMC 2023 February 01.

Published in final edited form as:

Glia. 2022 February ; 70(2): 321–336. doi:10.1002/glia.24108.

N-myc downstream regulated family member 1 (NDRG1) is enriched in myelinating oligodendrocytes and impacts myelin degradation in response to demyelination.

Damien Marechal[1], **David K. Dansu**[1,2], **Kamilah Castro**[1,3,*], **Julia Patzig**[1,**], **Laura Magri**[3,***], **Benjamin Inbar**[1], **Mar Gacias**[3,****], **Sarah Moyon**[1,*****], **Patrizia Casaccia**[1,2,3,4,#]

[1]Neuroscience Initiative, Advanced Science Research Center, CUNY, 85 St Nicholas Terrace, New York, NY 10031, USA

[2]Graduate Program in Biochemistry, The Graduate Center of The City University of New York, New York, NY 10016, USA

[3]Department of Neuroscience, Icahn School of Medicine at Mount Sinai, New York, NY 10029, USA

[4]Graduate Program in Biology, The Graduate Center of The City University of New York, New York, NY 10016, USA

Abstract

The *N-myc downstream regulated gene family member 1* (*NDRG1*) is a gene whose mutation results in peripheral neuropathy with central manifestations. While most of previous studies characterized NDRG1 role in Schwann cells, the detection of central nervous system symptoms and the identification of NDRG1 as a gene silenced in the white matter of Multiple Sclerosis brains raise the question regarding its role in oligodendrocytes. Here we show that NDRG1 is enriched in oligodendrocytes and myelin preparations, and we characterize its expression using a novel reporter mouse (*TgNdrg1-EGFP*). We report NDRG1 expression during developmental myelination and during remyelination after cuprizone-induced demyelination of the adult corpus callosum. The transcriptome of *Ndrg1-EGFP+* cells further supports the identification of late myelinating oligodendrocytes, characterized by expression of genes regulating lipid metabolism and bioenergetics. We also generate a lineage specific conditional knockout (*Olig1*$^{cre/+}$;*Ndrg1*$^{fl/fl}$) line to study its function. Null mice develop normally, and despite similar numbers of progenitor cells as wild type, they have fewer mature oligodendrocytes and lower levels of myelin proteins

#Corresponding author: pcasaccia@gc.cuny.edu.
*present address: ClinicalMind LLC, Long Island City, NY
**present address: Pfizer, Muenster, Germany
***present address: McCann Health, Milano, Italy
****present address: Ajuntament de Palma, Palma, Spain
*****present address: Neuroscience Institute and Department of Neuroscience and Physiology, NYU Grossman School of Medicine, New York, USA.

Conflict of Interest Statement: The authors declare no competing interests.

Authorship: PC was responsible for conceptualization, fund acquisition, overall supervision, writing of the manuscript together with SM and DM. Experimental data on reporter mice were initially performed by LM, MG, JP, KC. SM conducted sorting from *Ndrg1-EGFP* mouse brains, she was responsible for the RNA-Seq analysis and qRT-PCR validation and supervised with DM some of the experiments on cuprizone-induced demyelination. All the experiments on the knockout mice included in this manuscript were performed by DKD and DM, with the contribution of BI.

than controls, thereby suggesting NDRG1 as important for the maintenance of late myelinating oligodendrocytes. In addition, when control and *Ndrg1* null mice are subject to cuprizone-induced demyelination, we observe a higher degree of demyelination in the mutants. Together these data identify NDRG1 as an important molecule for adult myelinating oligodendrocytes, whose decreased levels in the normal appearing white matter of human MS brains may result in greater susceptibility of myelin to damage.

Graphical Abstract

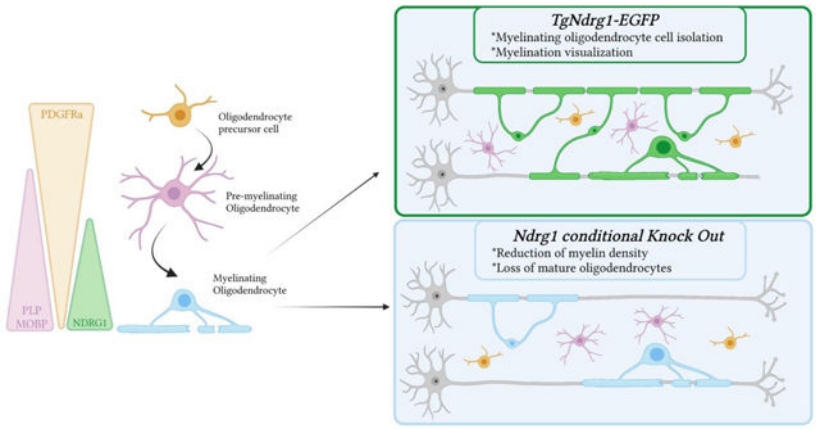

Keywords

brain; multiple sclerosis; epigenetic; repair

Introduction.

N-myc downstream regulated gene family member 1 (*NDRG1)* is a highly conserved and widely expressed gene, which has been extensively characterized in the peripheral nervous system. Its mutation has been causally linked to the severe demyelinating hereditary motor and sensory neuropathy Lom (Jahn et al., 2020; Kalaydjieva et al., 2000). This autosomal recessive form of the peripheral neuropathy Charcot Mary Tooth type 4D (CMT4D) has been linked to either mutations (Hunter et al., 2003) or intragenic duplications of exons 6 and 8 of the *NDRG1* gene, eventually leading to decreased levels of the transcript (Okamoto et al., 2014). Most of the previous studies of NDRG1 have focused on its role in the peripheral nerve, where it was mostly detected in mature myelinating Schwann cells (Berger, Sirkowski, Scherer, & Suter, 2004; Kalaydjieva et al., 2000; King et al., 2011). Peripheral nerves were characterized in two mouse models, including *"stretcher"* mice, with spontaneous deletion of *Ndrg1* exons 10 through 14 resulting in total NDRG1 deficiency in a BALB/c background (King et al., 2011) and in mice with systemic deletion of the first exon of *Ndrg1* in a C5BL/6 background (Okuda et al., 2004) both reported peripheral demyelination starting at 5 weeks of age, while some phenotypic differences between the two models were likely due to the effect of the genetic background.

Despite the overall interest in the characterization of NDRG1 in the PNS, the clinical presentation of CNS symptoms in CMT4D patients (Echaniz-Laguna et al., 2007) suggested a role in oligodendrocytes. Our previous study in the normal appearing white matter of Multiple Sclerosis (MS) brains, identified NDRG1 as one of the genes with the lowest transcript and protein levels (Huynh et al., 2014), although its characterization in CNS oligodendrocytes remains elusive. Consistent with other studies (Berger et al., 2004; Kalaydjieva et al., 2000; Okuda, Kokame, & Miyata, 2008), here we show that *Ndrg1* levels are enriched in myelinating cells and that its levels are regulated by DNA methylation. We also provide an immunophenotypic and transcriptional characterization of a novel transgenic reporter mouse (*TgNdrg1-EGFP)* which we have rederived. We also report defective maintenance of mature oligodendrocytes and myelin regenerative potential in mice lacking *Ndrg1* (*Olig1*$^{cre/+}$;*Ndrg1*$^{fl/fl}$). Overall, our data suggest an essential role for NDRG1 in oligodendroglial cells, particularly in late myelinating oligodendrocytes, during both developmental and adult myelination.

Methods

Animals.

All experiments were performed according to IACUC-approved protocols and mice were maintained in a temperature- and humidity-controlled facility on a 12-h light-dark cycle with food and water ad libitum. Mice from either sex were used for all the experiments, except for cuprizone treated animals, where females were used for immunohistochemistry and Luxol Fast Blue staining protocols, and males were used for western blot. Transgenic *TgNdrg1-EGFP* mice were generated at the Mouse Genetics and Gene Targeting Shared Resource Facility at Icahn School of Medicine at Mount Sinai, by recovering the cryo-preserved sperm of Tg(*Ndrg1*-EGFP)EQ125Gsat/Mmucd (RRID:MMRRC_011851-UCD), obtained from the Mutant Mouse Repository and Research Center (MMRRC), into C57BL/6. The original BAC construct (RP24–312F21) in which the EGFP reporter gene was inserted, immediately upstream of the coding sequence of *Ndrg1* gene, was generated by GENSAT (Rockefeller University) and donated to the MMRRC as part of the NINDS-NIH supported GENSAT project (Gong et al., 2003). Mice were bred as hemizygous.

Other reporter mice used in this study include: the *Pdgfra-H2B-EGFP* line to identify the nuclei of oligodendrocyte progenitors as a histoneH2B- EGFP fusion protein is expressed from the endogenous *Pdgfra* promoter (Klinghoffer, Hamilton, Hoch, & Soriano, 2002) (RRID:IMSR-_JAX:007669), the *Plp-EGFP* line (Le Bras et al., 2005; Spassky et al., 1998) and the *Cnp-EGFP*, line (Yuan et al., 2002) to study pre-myelinating oligodendrocytes.

To generate the *Ndrg1* conditional knockout model, we obtained two clones of targeted ES cells (clone EPD0199_4_H05 and clone EPD0199_4_A08) carrying the floxed *Ndrg1* allele [*Ndrg1*$^{tm2a(KOMP)Wtsi}$] in C57BL/6N from the KOMP repository at UC Davis. Those clones were characterized by the insertion of floxed cassettes flanking exons 6 and 7 (chr15:66,943,783–66,945,292) and were microinjected into blastocyst-stage embryos at the Mouse Genetics and Gene Targeting Core Facility at Icahn School of Medicine at Mount Sinai. The chimeras were back crossed into C57BL/6N mice and screened to identify germline transmission and then used for the generation of floxed lines. Lineage specific

knockout lines were generated by crossing *Ndrg1*$^{fl/fl}$ females with *Olig1* $^{tm1(cre)Rth/J}$ males heterozygous for cre (referred to *Olig1*$^{cre/+}$ in the manuscript) (RRID:IMSR_JAX:011105), to generate the conditional mutants (*Olig1*$^{cre/+}$;*Ndrg1*$^{fl/fl}$). Littermates with the genotype *Olig1*$^{+/+}$;*Ndrg1*$^{fl/fl}$ were used as controls in this study. Genotyping using the following primers allowed identification of wild-type (amplicon 654 bp), floxed (amplicon 831 bp) and recombined (amplicon 714 bp) *Ndrg1* alleles:

Ndrg1-F: AGGGACAGGTCCAGGTTTAAAGAG;

Ndrg1-ttR: GACCCTAGACAGAGACGATACGTG;

Ndrg1-recomb: TAGTGTGGCATTTCAGCACC.

Cuprizone treatment.

P60 reporter male and female mice were treated for six weeks with a 0.2% cuprizone diet (Harlan diet) or chow diet to follow demyelination effects, followed by an additional two weeks under chow diet, in order to follow remyelination (Koutsoudaki et al., 2009; Silvestroff, Bartucci, Pasquini, & Franco, 2012; Skripuletz, Gudi, Hackstette, & Stangel, 2011; Skripuletz et al., 2008). P60 control and conditional *Ndrg1* null mice were fed with a 0.2% cuprizone diet (Harlan diet) or regular chow diet for the three weeks. This experiment was repeated three times on different cohorts of mice, in order to obtain triplicates. Tissue sections for immunohistochemistry and Luxol Fast Blue staining experiments were generated from female perfused brains, and corpora callosa protein extracts from male brains were used for western blot.

Cell sorting.

Oligodendroglial lineage cells at different stages of differentiation (used for qRT-PCR experiments) were sorted using fluorescence-activated cell sorting of distinct reporter mouse lines. Premyelinating OL were sorted from *Cnp-EGFP* (Yuan et al., 2002) mice and from *Plp-EGFP* brains (Le Bras et al., 2005; Spassky et al., 1998) at multiple developmental time points. Progenitors were sorted from the brains of *Pdgfra-H2B-EGFP* (Klinghoffer et al., 2002) mice during development (P5) and in adulthood (P60). Myelinating OL were isolated from *TgNdrg1-EGFP* mice, generated by GENSAT and characterized in this study. Tissue was dissected in HBSS 1X (HBSS 10X (Invitrogen), 0.01 M HEPES buffer, 0.75% sodium bicarbonate (Invitrogen), and 1% penicillin/streptomycin) and mechanically dissociated. After enzymatic digestion using papain (30 μg/ml in DMEM-Glutamax, with 0.24 μg/ml L-cysteine and 40 μg/ml DNase I), cells were separated on a pre-formed Percoll density gradient before centrifugation for 15 min at 22,000 *g*. Cells were then collected and stained with propidium iodide (PI) for 2 min at room temperature (RT). In a second step, GFP-positive and PI-negative cells were sorted by fluorescence-activated cell sorting (FACS; Aria, Becton Dickinson) and collected in pure fetal bovine serum. Cells were washed twice in PBS 1X (PBS 10X, Invitrogen) and the dry cell pellets were frozen at −80°C.

DNA and RNA extraction.

DNA and RNA were isolated from the same pellet of cells sorted from the entire forebrain, using an AllPrep DNA/RNA Mini Kit (Qiagen) with on-column DNase treatment during the RNA isolation. Corpus callosum and spinal cord tissue RNA were isolated from three biological replicates for each age and conditioned using TRIzol (Invitrogen) extraction and isopropanol precipitation. RNA samples were resuspended in water and further purified with RNeasy columns with on- column DNase treatment (Qiagen). RNA purity was assessed by measuring the A260/A280 ratio using a NanoDrop, and RNA quality checked using an Agilent 2100 Bioanalyzer (Agilent Technologies). DNA quality was checked using a NanoDrop and a Qubit Fluorometric quantitation (Thermo Fisher).

DNA methylation analysis.

Differentially methylated regions were validated using MassARRAY EpiTYPER assays (Sequenom), as previously described (Huynh et al., 2014). Genomic DNA was sodium bisulfite-treated using an Methylamp DNA modification kit (EpiGentek). MassARRAY EpiTYPER primers were designed using EpiDesigner software and used to amplify DMRs:

Ndrg1_F: aggaagagagGATTTTTTAGAAGTTTTGGTTTTTGG;

Ndrg1_R: cagtaatacgactcactatagggagaaggctTCAAACAAATTTCATTTTACATCCC.

Quantitative real-time PCR.

For qRT-PCR, RNA was reverse-transcribed with qScript cDNA Supermix (Quanta) and performed using PerfeCTa SYBR Green FastMix, ROX (Quanta) at the ASRC Epigenomic Core. After normalization to the geometric mean of house-keeping genes (*Ppia*, *18S* and *36B4*) the average values for each transcript were calculated as based on the values obtained in all the samples included for each condition.

The following primers were used:

Mbp; F- ACACACGAGAACTACCCATTATGG and R- AGAAATGGACTACTGGGTTTTCATCT;

Mog: F- AAGAGGCAGCAATGGAGTTG and R- CACAAGTGCGATGAGAGTCAG;

Myrf: F- GGCAGAGCAAGACCAAGAAC and R- GCACCTTCTGGCACACAGTA;

Ndrg1: F- AGAGTTCGATGTTCAGGAGCAG and R- TGTCGTGATACGTGAGGATGAC;

Ndrg2: F- CTGTGTGGAGACACCTTATGGC and R- CCGAAACAGTGGCTGGAAGCAA;

Ndrg3: F- CCAGCACTTTGCTGTCTGTCAC and R- GTGAGAACAGGAGGCAGCATCT;

Ndrg4: F- CAGTGATGCTGGTAGTCGGAGA and R- GTTGTGTCACCTGAGGAAGACC;

Cspg4 F- ACAGACGCCTTTGTTCTGCT and R- CCCGAATCATTGTCTGTTCC;

Olig2: F- CCGAAGCAATGGGAGCAT and R- GGAGTGTTCAGCCAAAGAGTCA;

Pdgfra: F- TTGGTGCTGTTGGTGATTGT and R- TCCCATCTGGAGTCGTAAGG;

Ppia: F- CACAAACGGTTCCCAGTTTT and R- TTCCCAAAGACCACATGCTT;

18S: F- AGTCCCTGCCCTTTGTACACA and R- GATCCGAGGGCCTCACTAAAC;

36B4: F- GGACCCGAGAAGACCTCCTT and R- GATCCGAGGGCCTCACTAAAC.

Western Blot.

Mice were sacrificed and spinal cords were dissected on ice, before being immediately processed for protein extraction. Protein lysates (10 μg or 50 μg for PDGFRA) were separated by sodium dodecyl sulfate–polyacrylamide gel electrophoresis (SDS–PAGE) and transferred onto a PolyVinylidene DiFluoride (PVDF) (Millipore, Billerica, MA, USA) membrane using a buffer containing 25 mM Tris base, pH 8.3, 192 mM glycine, 20% (vol/vol) methanol for 1 h at 100 V at 4 °C. Membranes were blocked for 1 h in 10% Milk/0.1% Tween/TBS, then incubated overnight at 4 °C with the primary antibody diluted in 5% Milk/0.1% Tween/TBS. Antibodies used include: mouse anti-CNPase (Sternberger Inc., SMI-91, 1:20,000), mouse anti-MBP (Covance, SMI-99, 1:5000), rabbit anti-NDRG1 (Abcam, ab124689, 1:10,000), mouse anti-OLIG2 (Millipore, MABN50, 1:1,000), rabbit anti-PDGFRA (Cell signaling 3164S, 1:2,000) mouse anti-αTUBULIN (Calbiochem, CP06, 1:2000), mouse anti-β-ACTIN (Sigma, AC-15 A5441, 1:5,000). After rinsing with 0.1% Tween/TBS, membranes were incubated 1h at room temperature with the horseradish peroxidase conjugated secondary antibodies conjugated (Jackson Immunoresearch, 1:10,000) in 5% Milk/0.1% Tween/TBS. After rinsing, membranes were incubated with ECL (Amersham) for 3 min and then revealed. Quantification was carried out on three biological replicates per age, using ImageJ. Protein expression was normalized to αTUBULIN or β-ACTIN expression and compared to their respective expression levels in P1 samples if multiple time points were analyzed or to the average of wildtype samples if multiple genotypes were analyzed.

Myelin isolation.

A light-weight membrane fraction enriched for myelin was purified from mouse spinal cords by sucrose density centrifugation and osmotic shocks as described (Jahn et al., 2020; Larocca & Norton, 2007). Purified myelin was subjected to further high-salt and high-pH washing/centrifugation cycles as described previously (Werner et al., 2007).

Immunohistochemistry.

Adult animals were perfused with 4% paraformaldehyde and post-fixed overnight in the same solution at 4°C. Brains were dissected and either cryo-protected in sucrose solutions and frozen embedded in OCT for *TgNdrg1-EGFP* tissues, or embedded in paraffin for the analysis of the null mutant and control tissues. Immunohistochemistry was performed on 12μm coronal cryostat sections or 10μm paraffin sections. Cryostat sections were treated with antigen retrieval (citrate buffer, 0.01M, pH=6) at 60°C for 1 h. Following a deparaffinization protocol, paraffin sections were treated with antigen retrieval (citrate

buffer, 0.01M, pH=6) at buffer boiling point for 10 min. Slides were then incubated in blocking buffer (5% normal goat serum in PBS/Triton-X100 0.3%) for 1 hour at room temperature and then overnight at 4°C with the primary antibodies diluted in a similar blocking buffer (5% normal goat serum in PBS/Triton-X100 0.3%). After rinsing with PBS 1X, sections were incubated with the Alexa Fluor secondary antibodies and then washed with PBS 1X. Stained sections were cover-slipped in DAPI Fluoromount G mounting medium (Thermo Fisher) and images were acquired on a Zeiss LSM800 Fluorescence Microscope. Quantification was performed on three technical replicates for each biological samples (n=3). *Primary antibodies used:* rabbit anti-IBA1 (Wako, 019–19741, 1:250), rabbit anti-GFAP (DakoCytomation, Z0334, 1:500), mouse anti-MBP (Covance, SMI-99, 1:200), mouse anti-NeuN (Chemicon, MAB377, 1:200), mouse anti-CC1 (Millipore, OP80, 1:200), rabbit anti-OLIG2 (Millipore, AB9610, 1:500).

Luxol Fast Blue staining.

Adult *Olig1*$^{cre/+}$;*Ndrg1*$^{fl/fl}$ and *Olig*$^{+/+}$;*Ndrg1*$^{fl/fl}$ were perfused with 4% paraformaldehyde and post-fixed overnight in the same solution at 4°C. Brains were dissected and embedded in paraffin. Staining was performed on 10μm microtome coronal sections. Dried paraffin sections were first deparaffinized with three baths of xylene (10 min each), followed by three baths of 100% ethanol (10 min each). After 5 min hydration in 95% ethanol, the sections were incubated overnight in Luxol Fast blue solution (0.1%) at 50°C. Sections were rinsed 1 min in 95% ethanol and washed 5 min under running tap water. Sections were differentiated 7s in lithium carbonate (0.05%), washed three times in 70% ethanol (1 min, 1 min and 10 min), then 5 min under running tap water. Finally, sections were dehydrated with successively for 5 min in 70%, 95% and 100% ethanol. The procedure was concluded by three baths of xylene (10 min each) and sections were mounted with DPX mounting medium (Sigma-Aldrich). For each replicate, coronal imaging of the whole brain at one coordinate (Bregma −1.46mm) was obtained using a slide scanner (Leica Aperio CS2 slide scanner, objective 20x/0.75 NA Plan Apo). High magnification (x63) images of the corpus callosum region were obtained with the imager EVOS FL Auto 2 (Invitrogen) and quantified for each replicate using ImageJ. For each genotype and diet condition, 3 biological samples were analyzed.

RNA-Sequencing.

A total of 100ng of total RNA per sample was used for library construction using the Ultra-Low-RNA-seq RNA Sample Prep Kit (Illumina) and sequenced using the Illumina HiSeq 2500 instrument yielding 100 bp paired-end reads. High-quality reads were aligned to the mouse reference genome (mm10), RefSeq exons, splicing junctions, and contamination databases (ribosome and mitochondria sequences) were identified using the Burrows-Wheeler Aligner (BWA) algorithm. The read count for each RefSeq transcript was extracted using uniquely aligned reads to exon and splice-junction regions. The raw read counts were input into DESeq2 v1.2.5 (Anders & Huber, 2010), for normalizing the signal for each transcript and to ascertain differential gene expression with associated p-values. Hierarchical clustering of all samples and heatmap visualization were performed on Multi-Experiment Viewer. Specific OPC, OL, neuronal, astroglial, microglial and endothelial markers were identified using Zhang et al., 2014 database (Y. Zhang et al., 2014). We

computed hypergeometric p-values for over-representation of each biological process gene ontology (GO) category using GOrilla (Eden, Navon, Steinfeld, Lipson, & Yakhini, 2009).

Quantification and statistical analysis.

Image acquisition was performed on a Zeiss LSM800 Fluorescence Microscope, using ZEN software. Images were analyzed with Fiji-Image J (RRID:SCR_003070). All statistical analyses were done using GraphPad Prism (GraphPad Software, Inc, RRID:SCR_002798). Unpaired Student's t-test were used for every two datasets with equal variances and for which data followed a normal distribution. A one-way ANOVA with Tukey's post-hoc test was performed each time we had three samples or more, in order to identify the datasets driving the statistical significance. For data comparing different diets to the control chow we used a one-way ANOVA with Dunnett's post-hoc test. Two-way ANOVA, followed by a Tukey's post hoc test, was performed to compare four datasets comparing wild type and mutants either on chow or on cuprizone diet. For all graphs, error bars are represented as average ± SD. For all quantifications, n= 3–5 mice were examined; the specific number of mice used in each experiment is noted in the corresponding figure legends. The statistical details for each figure panel are listed in the Supplementary table 4.

Data and software availability.

Sequencing data have been deposited in the NCBI's Gene Expression Omnibus Series accession number GSE113614.

Results

NDRG1 expression in myelinating oligodendrocytes and white matter tracts.

NDRG1 is a well conserved gene that is expressed in several tissues (Schonkeren et al., 2019) and enriched in myelinating cells of the peripheral and central nervous system (Berger et al., 2004; King et al., 2011; Okuda et al., 2008). We became interested in characterizing this gene because its levels were significantly decreased in the normal appearing white matter of post-mortem multiple sclerosis (MS) human brains, due to DNA hypermethylation (Huynh et al., 2014). The mouse homologue of the human *NDRG1* gene is *Ndrg1,* whose transcript levels were found to increase as oligodendrocyte progenitors differentiate into oligodendrocytes (Moyon et al., 2016; Y. Zhang et al., 2014). As the low levels of the human NDRG1 protein in MS brains were associated with DNA hypermethylation of the human *NDRG1* gene, we asked whether the increased levels detected in mice during the differentiation of OPCs into OLs were consequent to hypomethylation at the murine *Ndrg1* locus (Figure 1A, orange locus). We used several mouse reporter lines to enrich for oligodendroglial lineage cells, at specific stages of differentiation. To enrich for oligodendrocyte progenitors we used the *Pdgfra-H2B-EGFP* line (Klinghoffer et al., 2002), expressing a histone H2B-EGFP protein from the endogenous *Pdgfra* promoter. To enrich for premyelinating oligodendrocytes we used two additional reporter knock-in lines: *Cnp-EGFP* (Yuan et al., 2002) and *Plp-EGFP* (Le Bras et al., 2005; Spassky et al., 1998). The methylation status of the *Ndrg1* locus during developmental myelination was assessed by testing DNA samples from neonatal oligodendrocyte progenitors, sorted from *Pdgfra-H2B-EGFP* brains at postnatal day 5 (P5), and oligodendrocytes, sorted from *Plp-EGFP*

brains at postnatal day 21 (P21). Methylation at individual CpGs within the murine *Ndrg1* region on chromosome 15 (Figure 1B) was quantified using MassARRAY EpiTyper, a mass spectrometry-based method which quantifies differences in specific cytosines after bisulfite conversion of DNA. This analysis revealed that five out of five CpGs within the *Ndrg1* locus were hypomethylated as progenitors differentiated into oligodendrocytes (Figure 1B). To further validate that hypomethylation was associated with transcriptional activation as cells differentiated into oligodendrocytes, we measured *Ndrg1* transcript levels in *Cnp-EGFP+* (Figure 1C) sorted premyelinating oligodendrocytes (Yuan et al., 2002), at several time points of developmental myelination. While *Ndrg1* was almost undetectable during the first postnatal week its levels started to rise as progenitors differentiate into oligodendrocytes and then dramatically increased during the formation of new myelin (Figure 1D). In contrast, the transcript levels of other family members such as *Ndrg2, Ndrg3* or *Ndrg4*, remained relatively low at all the time points analyzed (Figure 1D). These data were consistent with previously published transcriptomic data identifying *Ndrg1* as the major isoform expressed in myelinating oligodendrocytes with negligible expression of *Ndrg2–4* (Cahoy et al., 2008; Y. Zhang et al., 2014). A similar time course of *Ndrg1* expression was also detected when total RNA was isolated from corpus callosum or spinal cord tissue (Figure 1E). The earlier detection of *Ndrg1* transcripts in the spinal cord samples compared to corpus callosum was consistent with the caudal-to-rostral gradient of myelination. The increasing levels of NDRG1 in protein lysates from spinal cord tissue was also consistent with the accumulation of this protein during developmental myelination (Figure 1F–G). Since NDRG1 protein has previously been reported to be localized in the cytoplasm of Schwann cells and non-compact peripheral myelin (Berger et al., 2004), we compared its levels in protein lysates versus myelin preparations from adult mice enrichment, which revealed an average fold enrichment of 3.59 fold ± 0.21 in the myelin fraction (Figure 1H–I). This was of interest, as its enrichment in the myelin compartment was even greater than the enrichment reported for other myelin proteins such as CNP (average fold enrichment = 2.45 ± 0.17) or MBP (average fold enrichment = 2.13 ± 0.28) (Figure 1I). Together, these results identify NDRG1 as a specific component of myelinating oligodendrocytes.

Characterization of the *Ndrg1-EGFP* reporter mouse line.

To further characterize NDRG1 expression in the central nervous system, we generated a transgenic mouse, which we called *TgNdrg1-EGFP*, by cryo-recovering a BAC-EGFP based construct generated by GENSAT (see methods). The cell-type specificity of EGFP expression was validated in coronal brain sections of adult P60 mice by co-labeling the green fluorescent cells with antibodies specific for microglial (IBA1) (Figure 2A), astrocytic (GFAP) (Figure 2B), oligodendroglial (MBP) (Figure 2C) and neuronal (NeuN) markers (Figure 2D). Consistent with the western blot data showing NDRG1 enrichment in the myelin fraction, transgenic *TgNdrg1-EGFP* mice showed intense green fluorescence in white matter tracts of the adult brain (Figure 2A–D). *Ndrg1-EGFP* was co-expressed with MBP, confirming its specificity for the oligodendroglial lineage and its enrichment in myelinated tracts (Figure 2C). Importantly, EGFP signal was detected not only in myelinated fibers, but also in the cytoplasm of myelinating oligodendrocytes, thereby providing a useful somatic marker for counting and sorting them (Figure 2C). To further characterize NDRG1 expression during developmental myelination, sections were co-stained with antibodies for

the pan-oligodendroglial marker OLIG2 and for the differentiation marker recognized by the CC1 antibody, at multiple developmental time points (Figure 2E–G). In agreement with the pattern detected for NDRG1 in wild type mice, *Ndrg1-EGFP*+ cells were barely detectable in the postnatal day 10 brain (Figure 2E and 2H), but their number increased reaching an average percentage of 38.2 ±1.9 at postnatal day 16, of 58.8 ±2.1% at postnatal day 21 (Figure 2F–H). This increase correlated with the increased number of CC1+ oligodendrocytes whose percentage climbed from 29.3 ±0.7% at postnatal day 10 to 83.0 ±2.4% at postnatal day 21 (Figure 2E–G, 2I). Importantly, while all the *Ndrg1-EGFP*+ cells were also CC1+ (Figure 2J), the reverse was not true, as only an average percentage of 67.6 ±4.3% CC1+ cells expressed also NDRG1 at postnatal day 21 (Figure 2K). The enrichment of NDRG1 protein in the myelin fraction and the characterization of the green fluorescent cells in the newly generated *TgNdrg1-EGFP* reporter mice suggested NDRG1 as late marker of differentiated and myelinating oligodendrocytes.

The transcriptome of *Ndrg1-EGFP*+ cells is consistent with myelinating oligodendrocytes.

To address the molecular identity of cells sorted from P60 *TgNdrg1-EGFP* adult brains, we performed RNA-Sequencing analysis (Figure 3A). For comparative purposes, we also used datasets from adult progenitors (sorted from P60 *Pdgfrα-H2B-EGFP* reporter mice) and oligodendrocytes (sorted from P60 *Plp-EGFP* reporter mice) generated in our laboratory (Figure 3A). Following quality control, trimming, alignment of the reads to the murine genome (Table S1) and controlling for batch effects, the data were analyzed by using a three-dimensional principal component analysis (Figure 3B) and unsupervised hierarchical clustering of the three datasets (Figure 3C). Both analyses revealed the unique transcriptomic profile of each reporter line, which was consistent with the enrichment for cells at distinct stages of differentiation in the oligodendrocyte lineage cells, and with *TgNdrg1-EGFP*+ cells revealing a transcriptomic profile of late myelinating oligodendrocytes (Figure 3C). *Ndrg1*-EGFP+ cells sorted from the transgenic reporter mouse were enriched for myelin and oligodendroglial transcripts and did not express neuronal, astrocytic, microglial or endothelial lineage markers (Figure 3D), they were thereby reminiscent of the previously reported *Mobp-EGFP*+ reporter mice (Hughes, Orthmann-Murphy, Langseth, & Bergles, 2018; Kang et al., 2013). Of note, the similarity of the *TgNdrg1-EGFP* and *Mobp-EGFP*+ reporter mice was consistent with the interpretation that both mice are suitable reporter lines to label myelinating OL, although the expression of *Ndrg1* occurs after that of *Mobp* in several datasets (Li, Ruotti, Stewart, Thomson, & Dewey, 2010; Marques et al., 2016; Sharma et al., 2015). To define the unique gene ontology categories distinguishing the transcriptional profile of *Ndrg1*-EGFP+ myelinating oligodendrocytes from that of *Plp*-EGFP+ expressing pre-myelinating oligodendrocyte, we identified 803 upregulated (Table S2) and 2,318 down-regulated (Table S3) transcripts with a q-value <0.025 after FDR correction. Within the up-regulated gene ontology categories we detected lipid synthesis (e.g. *Chka/b, Cers2, Dctn6*), metabolism (e.g. *Aspa, Adk, Cb*) and bioenergetics (e.g. *Ndufs4, Surf1, Ndufa*) (Figure 3E), which is consistent with the previously reported role of NDRG1 and lipid metabolism in cancer cells (Sevinsky et al., 2018). Interestingly, the late myelinating NDRG1+ oligodendrocytes were less transcriptionally active than the PLP+ ones, as thousands of genes involved in transcriptional regulation regulating gene expression (e.g. *Hdac4, Nrxn1, Kmt*) and chromatin organization

(e.g. *Hdac4/11, Chd1, Ezh1*) were decreased at the later stages of oligodendrocytic differentiation (Figure 3F). Overall, this suggested that the transcriptional program of the late myelinating oligodendrocytes, isolated from the *TgNdrg1-EGFP* mice is consistent with cells with an active lipid metabolism, rather than transcriptional and epigenetic modulators of gene expression, which characterize the earlier stages.

Adult demyelination and remyelination using the *TgNdrg1-EGFP* reporter line.

As the *TgNdrg1-EGFP* reporter mouse line define a population of late myelinating OLs, we sought to test its potential utility in visualizing demyelination and remyelination in adult mice subject to the cuprizone model of demyelination. Therefore, we fed *TgNdrg1-EGFP* mice for 6 weeks with a 0.2% cuprizone diet and then we kept them for two weeks on a regular diet to favor remyelination (Figure 4A). In agreement with the demyelinating effect of the cuprizone diet, we detected the concomitant loss of MBP immunoreactivity and of the green fluorescence signal in the corpus callosum of transgenic mice on the cuprizone diet (Figure 4B). Remyelination was then assessed in transgenic mice that were allowed to recover on a chow diet for two additional weeks and showed recovery of green fluorescence in the corpus callosum, coincident with the restoration of MBP immunoreactivity in the callosal fibers (Figure 4B). Consistent with these immunohistological data, the transcript levels of *Ndrg1* in the corpus callosum decreased during the demyelination phase (6 wks) and increased during the repair phase (6 wks + 2 wks) (Figure 4C). Overall, these data indicate that the *TgNdrg1-EGFP* reporter mouse line represents a useful tool to successfully visualize and isolate mature mOLs from healthy and diseased adult brains.

Decreased number of oligodendrocytes and myelin proteins in lineage-specific *Ndrg1* mutants.

To define the functional role of NDRG1 in oligodendrocyte lineage cells, we generated lineage-specific conditional knock-out mice, by injecting engineered ES cells, generating chimeras and screening for germline transmission, as described in the methods. Conditional ablation in the oligodendrocyte lineage was then achieved by breeding these mice with *Olig1-cre* mice (Lu et al., 2002). The resulting $Olig1^{cre/+;}Ndrg1^{fl/fl}$ mice, were characterized by ablation of exons 6 and 7 of the murine *Ndrg1* gene, which correspond to the same exons carrying mutations in human patients with CMT4D and central neurological symptoms (Echaniz-Laguna et al., 2007; Okamoto et al., 2014) (Figure 5A). Prior to characterizing the knockout mice, we ascertained the effectiveness of the ablation by quantifying NDRG1 protein levels in lysates from the corpus callosum of adult P60 $Olig1^{cre/+;}Ndrg1^{fl/fl}$ mice and compared them to the levels in lysates from $Olig1^{+/+;}Ndrg1^{fl/fl}$ controls (Figure 5B–C). We confirmed that loss of *Ndrg1* was not compensated by up-regulation of any other family member and that the transcript levels of *Ndrg2*, *Ndrg3* and *Ndrg4* did not change between control and mutants (Figure 5D). We then measured several progenitor-selective (*Pdgfra* and *Cspg4)* and oligodendroglial specific (*Olig2, Myrf*, *Cnp*, *Mbp* and *Mog)* transcripts in RNA samples extracted from the adult corpus callosum of $Olig1^{cre/+;}Ndrg1^{fl/fl}$ mice and $Olig1^{+/+;}Ndrg1^{fl/fl}$ controls. While the transcript levels of the progenitor markers were not statistically different between the two genotypes (Figure 5E), the overall levels of mature OL markers were decreased (Figure 5F). Importantly, the levels of PDGFRα, a progenitor marker, were similar between the mice of the two genotypes, while the levels of OLIG2

protein, a marker for cells at all stages of the lineage, were down (Figure 5G–I) and were consistent with its lower transcript levels. The decreased number of mature OL without a corresponding increase of progenitor stage markers was suggestive of defective OL survival after genetic ablation of *Ndrg1,* rather than altered differentiation.

To further assess the role of NDRG1 in demyelinating conditions, we evaluated the effects of a short cuprizone feeding (3 weeks) in mutants and controls. Adult $Olig1^{cre/+};Ndrg1^{fl/fl}$ mutants and $Olig1^{+/+};Ndrg1^{fl/fl}$ controls were divided into two subgroups: one received a 0.2% cuprizone diet for 3 weeks and the other one was kept on a regular chow diet (Figure 6A). The effect of this demyelilnating insult on oligodendrocytes was evaluated by immunohistochemistry of the corpus callosum using the pan-lineage marker OLIG2+ and the differentiation marker CC1+ (Figure 6B). As expected, the starting number of OLIG2+ cells per mm^2 was lower in the mutants compared to control mice on a chow diet, and the numbers declined in mice of both genotypes on the cuprizone diet (Figure 6C). For both *Ndrg1* mutants and controls, a similar decrease in the percentage of OLIG2+ (Figure 6D) and CC1+ cells (Figure 6E–F) was observed in response to the demyelinating insult.

We also assessed the effect of cuprizone on the overall myelin protein levels by western blot analysis of protein extracts (Figure 6G–K) and by luxol fast blue staining of brain sections (Figure 6L–M). In agreement with the demyelinating effect of cuprizone the levels of the myelin proteins, CNPase and MBP were decreased in mice of both genotypes on the cuprizone diet, compared to chow fed mice. However the Ndrg1 mutant mice on a cuprizone diet showed an average 70% reduction for CNPase and MBP levels, which was substantially greater than the decrease induced by cuprizone diet in control mice (Figure 6I–K). These data highlighted the increased susceptibility of the *Ndrg1* mutant mice to cuprizone-induced demyelination. Staining of the myelin phospholipids, using Luxol Fast Blue (Figure 6L–M), after three weeks of cuprizone diet revealed less staining of the myelinated fibers although did not provide the sensitive quantitative assessment as the western blot analysis. Overall, we conclude that the absence of NDRG1 in oligodendrocytes may impact the stability of other myelin proteins and render them more susceptible to the effect of toxic stimuli.

Together these data support a functional role for NDRG1 in the maintenance of myelinating oligodendrocytes possibly by stabilizing myelin proteins and lipid enzymes. Reduction of NDRG1 levels has profound implication for the stability of myelinating cells in the adult brain and enhance their susceptibility to damage.

Discussion

This study, addressing the expression and function of NDRG1 in oligodendrocytes, was prompted by the identification of this gene as the most significantly downregulated in the unlesioned white matter of multiple sclerosis human brains compared to controls (Huynh et al., 2014). N-myc down-regulated gene 1 **(NDRG1)** is a highly conserved gene (Kalaydjieva et al., 2000), which is expressed at high levels in differentiated tissues and at low levels in proliferating and neoplastic cells, expressing c- MYC or N-MYC (Ellen, Ke, Zhang, & Costa, 2008; Magri et al., 2014; Melotte et al., 2010).In human gliomas, the levels of NDRG1 have been inversely correlated to tumor progression, with higher levels of

NDRG1 supporting longer patients' survival (Blaes et al., 2014) and low levels found in highly undifferentiated and metastatic cancers (B. Sun et al., 2009). These data suggested a function for NDRG1 as an anti-oncogene, which was further validated by the fact that its expression in cancer cells inhibited proliferation (Ma, Na, Tang, Wang, & Lin, 2015; A. H. Zhang et al., 2007) and metastatic dissemination (Maruyama et al., 2006), and favored apoptosis (Stein et al., 2004).

In physiological conditions, NDRG1 is highly expressed in the central and peripheral nervous system, where it is enriched in the cytoplasm of myelinating cells and in non-compact myelin (Berger et al., 2004). Mutations of *NDRG1* in humans have been causally linked to the onset of peripheral neuropathies, such as the Charcot Marie Tooth type 4D (CMT4D) (Berger, Young, & Suter, 2002; Kalaydjieva et al., 2000) and this spurred the interest in characterizing the function of this gene in the peripheral nerve. Using slightly different approaches, such as the generation of a total *Ndrg1* knockout mouse in C57Bl mice (Okuda et al., 2004) or in-frame deletion of exons 10 to 14 ("*stretcher*" mouse) to generate a truncated unstable transcript in Balb/b mice (King et al., 2011), two groups reported no effect on early developmental myelination, followed by a progressive demyelinating pathology, with a more severe phenotype in the *stretcher* mouse. Interestingly, in the peripheral nerve of these mice, myelin was normal until the onset of demyelination, which eventually resulted in axonal damage, especially of large caliber axons. It was therefore suggested that NDRG1 is crucial for peripheral nerve health by regulating trafficking and transport within the cytoplasm of Schwann cells, to meet the increasing demands of growing nerves. Unfortunately, however, neither one of these previous studies characterized central myelin. With the intent to address this gap of knowledge and motivated by the detection of low NDRG1 levels in MS brains (Huynh et al., 2014) and by reports of central symptoms in human subjects with a CMT4D diagnosis (Echaniz-Laguna et al., 2007; Kalaydjieva et al., 1998), we generated and characterized two novel mouse lines for the study of NDRG1 in oligodendrocyte lineage cells: a reporter line and an oligodendrocyte lineage specific knockout.

Based on a GENSAT construct with EGFP expression driven from the endogenous *Ndrg1* promoter, we generated a *TgNdrg1-EGFP* reporter mouse to study endogenous *Ndrg1* expression. In addition, by injection of ES cells characterized by the insertion of LoxP sites flanking exons 6 and 7 (obtained from UC Davis), we generated the *Ndrg1* $^{fl/fl}$ line, suitable for lineage specific ablation, upon breeding with specific *cre* lines. The detailed characterization of the immunophenotype and transcriptional profile of the EGFP+ cells in the *TgNdrg1-EGFP* reporter mouse revealed a temporal dynamic of NDRG1 expression *in vivo* which was consistent with the formation of white matter tracts during development and followed waves of demyelination or remyelination in the adult brain. The EGFP reporter expression was also consistent with the enrichment of the endogenous NDRG1 protein in myelin fractions from adult brain or spinal cord and its absence in progenitor cells was also consistent with the high levels of N-MYC expression in undifferentiated progenitors (Magri et al., 2014). Unbiased transcriptomic analysis of *Ndrg1-EGFP*+ cells sorted from the adult brain and compared to OL sorted from *Plp-EGFP* mice revealed a unique transcriptional signature characterized by higher levels of expression of genes regulating lipid metabolism and lower levels of transcripts encoding for transcription factors

or epigenomic modulators. Overall, these features identified NDRG1 as a very late marker of myelinating oligodendrocytes, an interpretation which is also in agreement with several reports of NDRG1 expression following that of *Mobp* (Marques et al., 2016).

Despite the general consensus on the identification of NDRG1 as marker of myelinating oligodendrocytes, its function remains not well defined and for this reason, we rederived a floxed Ndrg1 line and crossed it with a lineage specific cre driver, to generate *Olig1*$^{cre/+}$:*Ndrg1*$^{fl/fl}$ mice, lacking exons 6 and 7 of the murine gene, corresponding to the same regions in human patients with CMT4D and central neurological symptoms (Echaniz-Laguna et al., 2007; Okamoto et al., 2014). Previous studies on NDRG1 in cancer cells, suggested a role in promoting growth arrest (Ma et al., 2015; A. H. Zhang et al., 2007), differentiation (Fotovati et al., 2011), apoptosis (Stein et al., 2004) and arrest of metastasis (Maruyama et al., 2006). However, we and others have shown that NDRG1 is mostly expressed in post-mitotic, fully differentiated myelinating cells (Berger et al., 2004) and the phenotype of the *Ndrg1* null mouse line did not support a role for NDRG1 in regulating proliferation or apoptosis of either oligodendrocytes or Schwann cells. In addition, decreased levels of specific myelin proteins and fewer number of mature oligodendrocytes in the absence of accumulation of progenitor cells did not support the concept of defective differentiation, but rather a slow and progressive decay of differentiated OL. A potential explanation for such a phenotype, was suggested by *in vitro* studies in immortalized oligodendrocyte progenitor cell lines, which proposed a role for NDRG1 in lipid homeostasis and subcellular transport (King et al., 2011; Pietiäinen et al., 2013). Silencing of NDRG1 in Oli-Neu cells profoundly impacted the intracellular transport of cholesterol, leading to accumulation of ceramides and alteration in lipid metabolism. This concept is consistent with data in the peripheral nerve, where normal myelin formation was followed by demyelination (King et al., 2011). It is also supported by the unique transcriptomic signature of NDRG1+ cells, which revealed upregulation of genes regulating lipid metabolism. We therefore suggest that NDRG1 is a protein enriched in non-compact myelin, where it maintains homeostatic control of lipid/myelin proteins balance. To further test the putative functional role of NDRG1, we characterized *Ndrg1* null mice for normal development and then tested the effect of a demyelinating insult (cuprizone). *Ndrg1* null mice develop normally, they have similar number of oligodendrocyte progenitors, but fewer number of myelinating oligodendrocytes and less myelin than control, thereby suggesting that NDRG1 function does not affect differentiation, but rather the stability of the myelinating cells. In response to cuprizone, *Ndrg1* null male mice show a greater percent decrease of myelin proteins than controls, although the proportion of OLIG2+ cells was similarly decreased in mice of both genotypes. Although no sex differences were investigated and few mice of either sex were used for this study, our results suggest that NDRG1 regulates the stability of myelin proteins. In its absence, myelin proteins appear to become more sensitive to turnover (during normal development) or degradation (in response to demyelinating signals like cuprizone). These data, at least in part, explain the lower levels of myelin proteins detected in the corpus callosum of *Ndrg1* null mice, although future studies will be needed to further highlight the mechanism of regulation of myelin protein stability.

Besides the control of *Ndrg1* transcript levels, in response to several stressors (Cangul, 2004; B. Chen, Nelson, & Sadovsky, 2006; Z. Chen et al., 2012; Dixon et al., 2013; Le & Richardson, 2004; J. Sun et al., 2013), the cellular availability of the NDRG1 protein is also regulated by post-transcriptional modifications, including phosphorylation and sumoylation. NDRG1 can be phosphorylated by several protein kinases (García-Martínez & Alessi, 2008; McCaig, Potter, Abramczyk, & Murray, 2011) known to be responsive to external stimuli, such as nutrients and growth factors (Hay & Sonenberg, 2004). It can also be SUMOylated by SUMO-2 (Lee & Kim, 2015), whose activity is regulated by cellular stressors, such as DNA damage, viral infection, ER stress, and nutrient status (Enserink, 2015). Together, these data suggest that NDRG1 in oligodendrocytes may serve as a molecular interface, between external factors and myelin proteins. This is of particular importance in pathological conditions, when myelin stability is challenged by external factors, including autoimmune attacks.

Supplementary Material

Refer to Web version on PubMed Central for supplementary material.

Acknowledgements:

This work was supported by grants: R35-NS111604 from the National Institute of Health and RG-4890 from the National Multiple Sclerosis Society to PC; a PhD fellowships from NIH (5F31NS098575) to KC and from postdoctoral fellowships from the Paralyzed Veterans of America (3061) and National Multiple Sclerosis Society (FG-1507–04996) to SM. The initial study was also in part supported by postdoctoral fellowships FG-1804–30361 to JP and FG-2070 to LM. We acknowledge “The Gene Expression Nervous System Atlas” (GENSAT) Project, NINDS Contracts N01NS02331 & HHSN271200723701C to The Rockefeller University (New York, NY) for the generation of the BAC-EGFP transgenic construct.

REFERENCES

Anders S, & Huber W. (2010). Differential expression analysis for sequence count data. Genome Biol, 11(10), R106. doi:10.1186/gb-2010-11-10-r106 [PubMed: 20979621]

Berger P, Sirkowski EE, Scherer SS, & Suter U. (2004). Expression analysis of the N-Myc downstream-regulated gene 1 indicates that myelinating Schwann cells are the primary disease target in hereditary motor and sensory neuropathy-Lom. Neurobiol Dis, 17(2), 290–299. doi:10.1016/j.nbd.2004.07.014 [PubMed: 15474366]

Berger P, Young P, & Suter U. (2002). Molecular cell biology of Charcot-Marie-Tooth disease. Neurogenetics, 4(1), 1–15. doi:10.1007/s10048-002-0130-z [PubMed: 12030326]

Blaes J, Weiler M, Sahm F, Hentschel B, Osswald M, Czabanka M, … Wick W. (2014). NDRG1 prognosticates the natural course of disease in WHO grade II glioma. J Neurooncol, 117(1), 25–32. doi:10.1007/s11060-013-1357-2 [PubMed: 24395351]

Cahoy JD, Emery B, Kaushal A, Foo LC, Zamanian JL, Christopherson KS, … Barres BA (2008). A transcriptome database for astrocytes, neurons, and oligodendrocytes: a new resource for understanding brain development and function. J Neurosci, 28(1), 264–278. doi:10.1523/jneurosci.4178-07.2008 [PubMed: 18171944]

Cangul H. (2004). Hypoxia upregulates the expression of the NDRG1 gene leading to its overexpression in various human cancers. BMC Genet, 5, 27. doi:10.1186/1471-2156-5-27 [PubMed: 15341671]

Chen B, Nelson DM, & Sadovsky Y. (2006). N-myc down-regulated gene 1 modulates the response of term human trophoblasts to hypoxic injury. J Biol Chem, 281(5), 2764–2772. doi:10.1074/jbc.M507330200 [PubMed: 16314423]

Chen Z, Zhang D, Yue F, Zheng M, Kovacevic Z, & Richardson DR (2012). The iron chelators Dp44mT and DFO inhibit TGF-β-induced epithelial-mesenchymal transition via up-regulation of N-Myc downstream-regulated gene 1 (NDRG1). J Biol Chem, 287(21), 17016–17028. doi:10.1074/jbc.M112.350470 [PubMed: 22453918]

Dixon KM, Lui GY, Kovacevic Z, Zhang D, Yao M, Chen Z, … Richardson DR (2013). Dp44mT targets the AKT, TGF-β and ERK pathways via the metastasis suppressor NDRG1 in normal prostate epithelial cells and prostate cancer cells. Br J Cancer, 108(2), 409–419. doi:10.1038/bjc.2012.582 [PubMed: 23287991]

Echaniz-Laguna A, Degos B, Bonnet C, Latour P, Hamadouche T, Lévy N, & Leheup B. (2007). NDRG1-linked Charcot-Marie-Tooth disease (CMT4D) with central nervous system involvement. Neuromuscul Disord, 17(2), 163–168. doi:10.1016/j.nmd.2006.10.002 [PubMed: 17142040]

Eden E, Navon R, Steinfeld I, Lipson D, & Yakhini Z. (2009). GOrilla: a tool for discovery and visualization of enriched GO terms in ranked gene lists. BMC Bioinformatics, 10, 48. doi:10.1186/1471-2105-10-48 [PubMed: 19192299]

Ellen TP, Ke Q, Zhang P, & Costa M. (2008). NDRG1, a growth and cancer related gene: regulation of gene expression and function in normal and disease states. Carcinogenesis, 29(1), 2–8. doi:10.1093/carcin/bgm200 [PubMed: 17916902]

Enserink JM (2015). Sumo and the cellular stress response. Cell Div, 10, 4. doi:10.1186/s13008-015-0010-1 [PubMed: 26101541]

Fotovati A, Abu-Ali S, Kage M, Shirouzu K, Yamana H, & Kuwano M. (2011). N-myc downstream-regulated gene 1 (NDRG1) a differentiation marker of human breast cancer. Pathol Oncol Res, 17(3), 525–533. doi:10.1007/s12253-010-9342-y [PubMed: 21221878]

García-Martínez JM, & Alessi DR (2008). mTOR complex 2 (mTORC2) controls hydrophobic motif phosphorylation and activation of serum- and glucocorticoid-induced protein kinase 1 (SGK1). Biochem J, 416(3), 375–385. doi:10.1042/bj20081668 [PubMed: 18925875]

Gong S, Zheng C, Doughty ML, Losos K, Didkovsky N, Schambra UB, … Heintz N. (2003). A gene expression atlas of the central nervous system based on bacterial artificial chromosomes. Nature, 425(6961), 917–925. doi:10.1038/nature02033 [PubMed: 14586460]

Hay N, & Sonenberg N. (2004). Upstream and downstream of mTOR. Genes Dev, 18(16), 1926–1945. doi:10.1101/gad.1212704 [PubMed: 15314020]

Hughes EG, Orthmann-Murphy JL, Langseth AJ, & Bergles DE (2018). Myelin remodeling through experience-dependent oligodendrogenesis in the adult somatosensory cortex. Nat Neurosci, 21(5), 696–706. doi:10.1038/s41593-018-0121-5 [PubMed: 29556025]

Hunter M, Bernard R, Freitas E, Boyer A, Morar B, Martins IJ, … Kalaydjieva L. (2003). Mutation screening of the N-myc downstream-regulated gene 1 (NDRG1) in patients with Charcot-Marie-Tooth Disease. Hum Mutat, 22(2), 129–135. doi:10.1002/humu.10240 [PubMed: 12872253]

Huynh JL, Garg P, Thin TH, Yoo S, Dutta R, Trapp BD, … Casaccia P. (2014). Epigenome-wide differences in pathology-free regions of multiple sclerosis-affected brains. Nat Neurosci, 17(1), 121–130. doi:10.1038/nn.3588 [PubMed: 24270187]

Jahn O, Siems SB, Kusch K, Hesse D, Jung RB, Liepold T, … Werner HB (2020). The CNS Myelin Proteome: Deep Profile and Persistence After Post-mortem Delay. Front Cell Neurosci, 14, 239. doi:10.3389/fncel.2020.00239 [PubMed: 32973451]

Kalaydjieva L, Gresham D, Gooding R, Heather L, Baas F, de Jonge R, … Thomas PK (2000). N-myc downstream-regulated gene 1 is mutated in hereditary motor and sensory neuropathy-Lom. Am J Hum Genet, 67(1), 47–58. doi:10.1086/302978 [PubMed: 10831399]

Kalaydjieva L, Nikolova A, Turnev I, Petrova J, Hristova A, Ishpekova B, … Thomas PK (1998). Hereditary motor and sensory neuropathy--Lom, a novel demyelinating neuropathy associated with deafness in gypsies. Clinical, electrophysiological and nerve biopsy findings. Brain, 121 (Pt 3), 399–408. doi:10.1093/brain/121.3.399 [PubMed: 9549516]

Kang SH, Li Y, Fukaya M, Lorenzini I, Cleveland DW, Ostrow LW, … Bergles DE (2013). Degeneration and impaired regeneration of gray matter oligodendrocytes in amyotrophic lateral sclerosis. Nat Neurosci, 16(5), 571–579. doi:10.1038/nn.3357 [PubMed: 23542689]

King RH, Chandler D, Lopaticki S, Huang D, Blake J, Muddle JR, … Kalaydjieva L. (2011). Ndrg1 in development and maintenance of the myelin sheath. Neurobiol Dis, 42(3), 368–380. doi:10.1016/j.nbd.2011.01.030 [PubMed: 21303696]

Klinghoffer RA, Hamilton TG, Hoch R, & Soriano P. (2002). An allelic series at the PDGFalphaR locus indicates unequal contributions of distinct signaling pathways during development. Dev Cell, 2(1), 103–113. doi:10.1016/s1534-5807(01)00103-4 [PubMed: 11782318]

Koutsoudaki PN, Skripuletz T, Gudi V, Moharregh-Khiabani D, Hildebrandt H, Trebst C, & Stangel M. (2009). Demyelination of the hippocampus is prominent in the cuprizone model. Neurosci Lett, 451(1), 83–88. doi:10.1016/j.neulet.2008.11.058 [PubMed: 19084049]

Larocca JN, & Norton WT (2007). Isolation of myelin. Curr Protoc Cell Biol, Chapter 3, Unit3.25. doi:10.1002/0471143030.cb0325s33

Le Bras B, Chatzopoulou E, Heydon K, Martínez S, Ikenaka K, Prestoz L, … Thomas JL (2005). Oligodendrocyte development in the embryonic brain: the contribution of the plp lineage. Int J Dev Biol, 49(2–3), 209–220. doi:10.1387/ijdb.041963bl [PubMed: 15906234]

Le NT, & Richardson DR (2004). Iron chelators with high antiproliferative activity up-regulate the expression of a growth inhibitory and metastasis suppressor gene: a link between iron metabolism and proliferation. Blood, 104(9), 2967–2975. doi:10.1182/blood-2004-05-1866 [PubMed: 15251988]

Lee JE, & Kim JH (2015). SUMO modification regulates the protein stability of NDRG1. Biochem Biophys Res Commun, 459(1), 161–165. doi:10.1016/j.bbrc.2015.02.090 [PubMed: 25712528]

Li B, Ruotti V, Stewart RM, Thomson JA, & Dewey CN (2010). RNA-Seq gene expression estimation with read mapping uncertainty. Bioinformatics, 26(4), 493–500. doi:10.1093/bioinformatics/btp692 [PubMed: 20022975]

Lu QR, Sun T, Zhu Z, Ma N, Garcia M, Stiles CD, & Rowitch DH (2002). Common developmental requirement for Olig function indicates a motor neuron/oligodendrocyte connection. Cell, 109(1), 75–86. doi:10.1016/s0092-8674(02)00678-5 [PubMed: 11955448]

Ma W, Na M, Tang C, Wang H, & Lin Z. (2015). Overexpression of N-myc downstream-regulated gene 1 inhibits human glioma proliferation and invasion via phosphoinositide 3-kinase/AKT pathways. Mol Med Rep, 12(1), 1050–1058. doi:10.3892/mmr.2015.3492 [PubMed: 25777142]

Magri L, Gacias M, Wu M, Swiss VA, Janssen WG, & Casaccia P. (2014). c-Myc-dependent transcriptional regulation of cell cycle and nucleosomal histones during oligodendrocyte differentiation. Neuroscience, 276, 72–86. doi:10.1016/j.neuroscience.2014.01.051 [PubMed: 24502923]

Marques S, Zeisel A, Codeluppi S, van Bruggen D, Mendanha Falcão A, Xiao L, … Castelo-Branco G. (2016). Oligodendrocyte heterogeneity in the mouse juvenile and adult central nervous system. Science, 352(6291), 1326–1329. doi:10.1126/science.aaf6463 [PubMed: 27284195]

Maruyama Y, Ono M, Kawahara A, Yokoyama T, Basaki Y, Kage M, … Kuwano M. (2006). Tumor growth suppression in pancreatic cancer by a putative metastasis suppressor gene Cap43/NDRG1/Drg-1 through modulation of angiogenesis. Cancer Res, 66(12), 6233–6242. doi:10.1158/0008-5472.CAN-06-0183 [PubMed: 16778198]

McCaig C, Potter L, Abramczyk O, & Murray JT (2011). Phosphorylation of NDRG1 is temporally and spatially controlled during the cell cycle. Biochem Biophys Res Commun, 411(2), 227–234. doi:10.1016/j.bbrc.2011.06.092 [PubMed: 21708134]

Melotte V, Qu X, Ongenaert M, van Criekinge W, de Bruïne AP, Baldwin HS, & van Engeland M. (2010). The N-myc downstream regulated gene (NDRG) family: diverse functions, multiple applications. FASEB J, 24(11), 4153–4166. doi:10.1096/fj.09-151464 [PubMed: 20667976]

Moyon S, Huynh JL, Dutta D, Zhang F, Ma D, Yoo S, … Casaccia P. (2016). Functional Characterization of DNA Methylation in the Oligodendrocyte Lineage. Cell Rep, 15(4), 748–760. doi:10.1016/j.celrep.2016.03.060 [PubMed: 27149841]

Okamoto Y, Goksungur MT, Pehlivan D, Beck CR, Gonzaga-Jauregui C, Muzny DM, … Lupski JR (2014). Exonic duplication CNV of NDRG1 associated with autosomal-recessive HMSN-Lom/CMT4D. Genet Med, 16(5), 386–394. doi:10.1038/gim.2013.155 [PubMed: 24136616]

Okuda T, Higashi Y, Kokame K, Tanaka C, Kondoh H, & Miyata T. (2004). Ndrg1-deficient mice exhibit a progressive demyelinating disorder of peripheral nerves. Mol Cell Biol, 24(9), 3949–3956. doi:10.1128/mcb.24.9.3949-3956.2004 [PubMed: 15082788]

Okuda T, Kokame K, & Miyata T. (2008). Differential expression patterns of NDRG family proteins in the central nervous system. J Histochem Cytochem, 56(2), 175–182. doi:10.1369/jhc.7A7323.2007 [PubMed: 17998568]

Pietiäinen V, Vassilev B, Blom T, Wang W, Nelson J, Bittman R, … Ikonen E. (2013). NDRG1 functions in LDL receptor trafficking by regulating endosomal recycling and degradation. J Cell Sci, 126(Pt 17), 3961–3971. doi:10.1242/jcs.128132 [PubMed: 23813961]

Schonkeren SL, Massen M, van der Horst R, Koch A, Vaes N, & Melotte V. (2019). Nervous NDRGs: the N-myc downstream-regulated gene family in the central and peripheral nervous system. Neurogenetics, 20(4), 173–186. doi:10.1007/s10048-019-00587-0 [PubMed: 31485792]

Sevinsky CJ, Khan F, Kokabee L, Darehshouri A, Maddipati KR, & Conklin DS (2018). NDRG1 regulates neutral lipid metabolism in breast cancer cells. Breast Cancer Res, 20(1), 55. doi:10.1186/s13058-018-0980-4 [PubMed: 29898756]

Sharma K, Schmitt S, Bergner CG, Tyanova S, Kannaiyan N, Manrique-Hoyos N, … Simons M. (2015). Cell type- and brain region-resolved mouse brain proteome. Nat Neurosci, 18(12), 1819–1831. doi:10.1038/nn.4160 [PubMed: 26523646]

Silvestroff L, Bartucci S, Pasquini J, & Franco P. (2012). Cuprizone-induced demyelination in the rat cerebral cortex and thyroid hormone effects on cortical remyelination. Exp Neurol, 235(1), 357–367. doi:10.1016/j.expneurol.2012.02.018 [PubMed: 22421533]

Skripuletz T, Gudi V, Hackstette D, & Stangel M. (2011). De- and remyelination in the CNS white and grey matter induced by cuprizone: the old, the new, and the unexpected. Histol Histopathol, 26(12), 1585–1597. doi:10.14670/hh-26.1585 [PubMed: 21972097]

Skripuletz T, Lindner M, Kotsiari A, Garde N, Fokuhl J, Linsmeier F, … Stangel M. (2008). Cortical demyelination is prominent in the murine cuprizone model and is strain-dependent. Am J Pathol, 172(4), 1053–1061. doi:10.2353/ajpath.2008.070850 [PubMed: 18349131]

Spassky N, Goujet-Zalc C, Parmantier E, Olivier C, Martinez S, Ivanova A, … Thomas JL (1998). Multiple restricted origin of oligodendrocytes. J Neurosci, 18(20), 8331–8343. [PubMed: 9763477]

Stein S, Thomas EK, Herzog B, Westfall MD, Rocheleau JV, Jackson RS, … Liang P. (2004). NDRG1 is necessary for p53-dependent apoptosis. J Biol Chem, 279(47), 48930–48940. doi:10.1074/jbc.M400386200 [PubMed: 15377670]

Sun B, Chu D, Li W, Chu X, Li Y, Wei D, & Li H. (2009). Decreased expression of NDRG1 in glioma is related to tumor progression and survival of patients. J Neurooncol, 94(2), 213–219. doi:10.1007/s11060-009-9859-7 [PubMed: 19337694]

Sun J, Zhang D, Bae DH, Sahni S, Jansson P, Zheng Y, … Richardson DR (2013). Metastasis suppressor, NDRG1, mediates its activity through signaling pathways and molecular motors. Carcinogenesis, 34(9), 1943–1954. doi:10.1093/carcin/bgt163 [PubMed: 23671130]

Werner HB, Kuhlmann K, Shen S, Uecker M, Schardt A, Dimova K, … Nave KA (2007). Proteolipid protein is required for transport of sirtuin 2 into CNS myelin. J Neurosci, 27(29), 7717–7730. doi:10.1523/jneurosci.1254-07.2007 [PubMed: 17634366]

Yuan X, Chittajallu R, Belachew S, Anderson S, McBain CJ, & Gallo V. (2002). Expression of the green fluorescent protein in the oligodendrocyte lineage: a transgenic mouse for developmental and physiological studies. J Neurosci Res, 70(4), 529–545. doi:10.1002/jnr.10368 [PubMed: 12404507]

Zhang AH, Rao JN, Zou T, Liu L, Marasa BS, Xiao L, … Wang JY (2007). p53-dependent NDRG1 expression induces inhibition of intestinal epithelial cell proliferation but not apoptosis after polyamine depletion. Am J Physiol Cell Physiol, 293(1), C379–389. doi:10.1152/ajpcell.00547.2006 [PubMed: 17442733]

Zhang Y, Chen K, Sloan SA, Bennett ML, Scholze AR, O'Keeffe S, … Wu JQ (2014). An RNA-sequencing transcriptome and splicing database of glia, neurons, and vascular cells of the cerebral cortex. J Neurosci, 34(36), 11929–11947. doi:10.1523/jneurosci.1860-14.2014 [PubMed: 25186741]

Main Points

- *NDRG1* is a gene regulated by DNA methylation in oligodendrocytes
- *Ndrg1-EGFP* reporter mice label oligodendrocytes in developing and adult brains
- *Ndrg1* null mice show increased myelin loss after cuprizone treatment

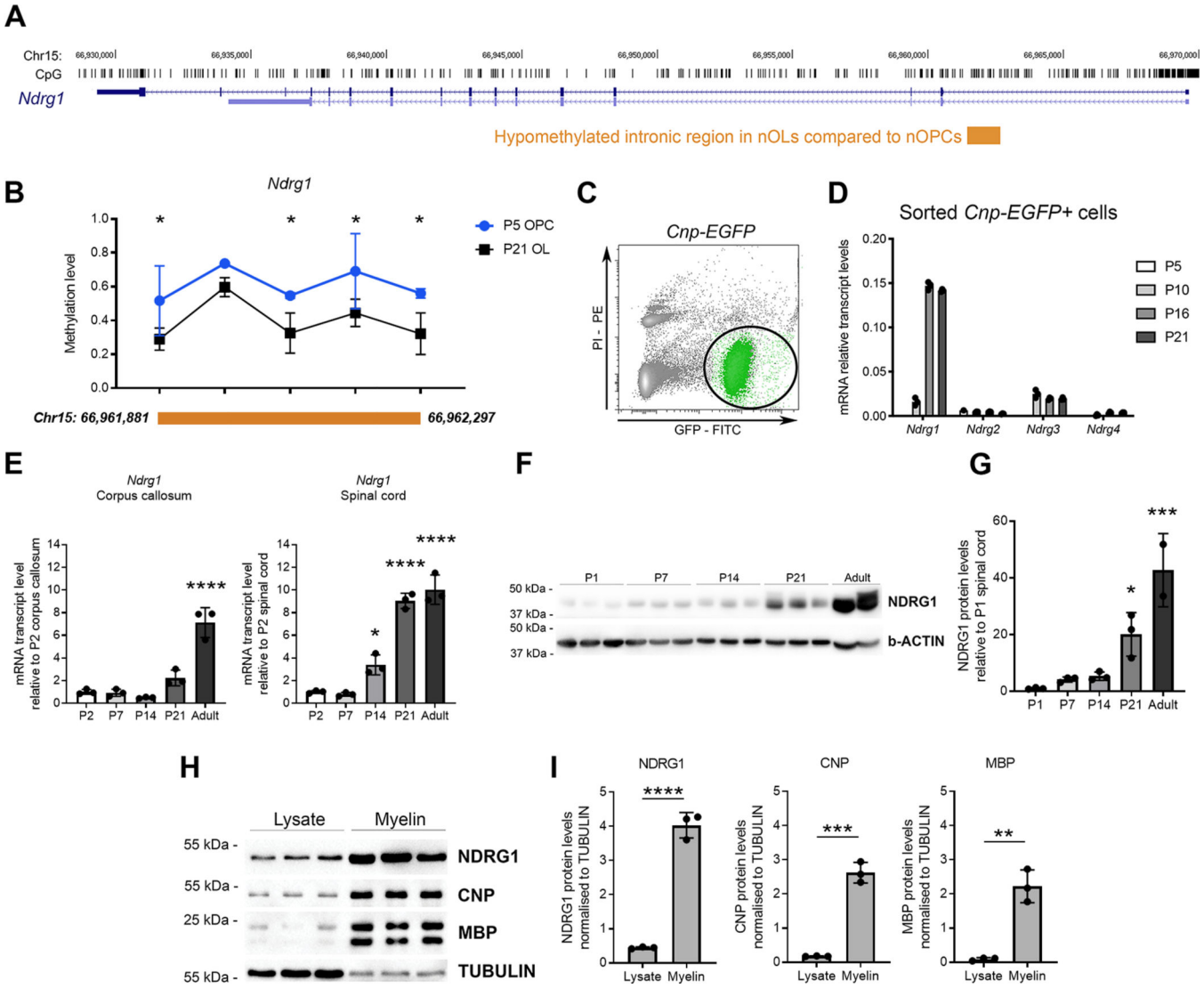

Figure 1. NDRG1 expression in myelinating oligodendrocytes and white matter tracts.

(**A**) Complete *Ndrg1* (in blue) murine gene structure from the UCSC Genome Browser including all the CpG island present on Chromosome 15 (black lines) and the DNA region regulated by DNA methylation in oligodendrocytes (in orange). (**B**) Methylation of individual CpGs in the *Ndrg1* locus (orange, corresponding to same region in A) assessed using MassARRAY EpiTYPER. DNA was isolated from postnatal day 5 progenitors (P5 OPC) from *Pdgfra-H2B-EGFP*+ mice (in blue) and from postnatal day 21 oligodendrocytes (P21 OL) sorted from the brain of *Plp-EGFP*+ mice (in black). Data represents average values ± SD for n=3–4 samples (*$p < 0.05$, multiple t-tests). (**C**) Representative fluorescence-activated cell sorting plot of sorted oligodendroglial cells, isolated from the spinal cords of *Cnp-EGFP*+ mice at P21. (**D**) Quantitative real-time PCR analysis of *Ndrg1*, *Ndrg2*, *Ndrg3* and *Ndrg4* transcripts in oligodendrocyte lineage sorted cells from spinal cord samples of *Cnp-EGFP*+ mice at P5, P10, P16 and P21. Data represents average values ± SD for n=3 samples. (**E**) Quantitative real-time PCR analysis of *Ndrg1* transcript levels in adult P60 corpus callosum and spinal cord tissue. Data represents average values ± SD for

n=3 samples (*$p < 0.05$, and ****$p < 0.0001$, one-way ANOVA, Tukey's post-hoc test). (**F**) Representative western blot of NDRG1 and β-ACTIN in spinal cord lysates during development. (**G**) Quantification of NDRG1 protein levels in spinal cord lysates at the indicated time points. Data were normalized to β-ACTIN and expressed as relative to the levels detected at P1. Data represents average values ± SD for n=3 samples, except for adult extracts n=2 (*$p < 0.05$ and ***$p < 0.001$, one-way ANOVA, Tukey's post-hoc test). (**H**) Representative western blot of NDRG1, CNP, MBP and TUBULIN in adult spinal cords total lysate and myelin-enriched fractions. (**I**) Quantification of NDRG1, CNP and MBP protein levels, normalized to TUBULIN. Data represents average values ± SD for n=3 samples **$p < 0.01$, ***$p < 0.001$ and ****$p < 0.0001$ unpaired t-test).

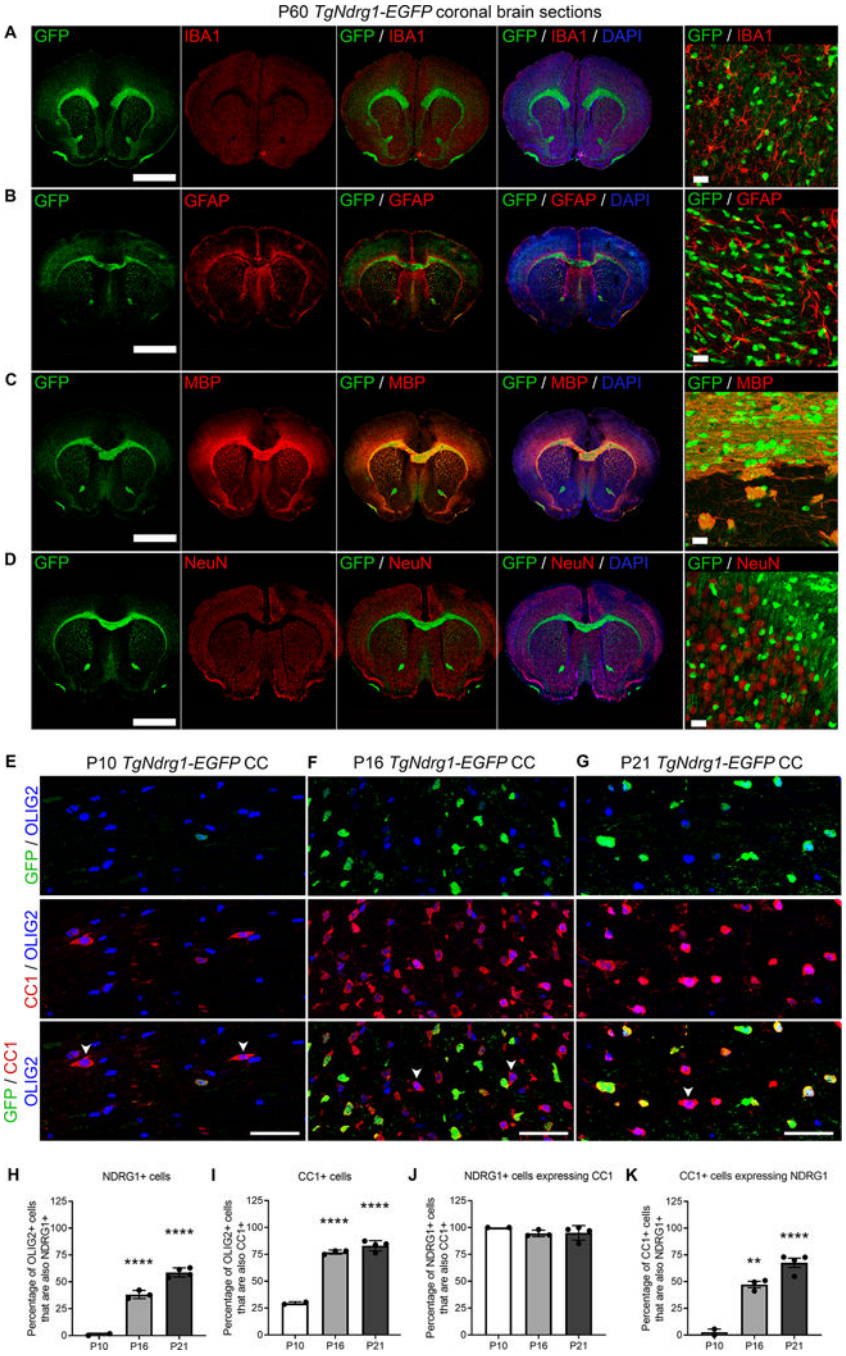

Figure 2. Spatial and temporal characterization of the *TgNdrg1-EGFP* reporter expression.

(**A**–**D**) Representative coronal brain sections obtained from adult P60 *TgNdrg1-EGFP* mice showing the green fluorescence from the reporter and the co-expression (red) with the microglial marker IBA1 (**A**), the astrocytic marker GFAP (**B**), the oligodendroglial marker MBP (**C**) and the neuronal marker NeuN (**D**). Note the unique and specific co-expression of NDRG1 with the oligodendroglial marker. Scale bar = 2mm. High magnification panels on the right, scale bar = 20μm. (**E**–**G**) Representative coronal brain sections from *TgNdrg1-EGFP* reporter mice at multiple time points, including P10 (**E**), P16 (**F**) and P21 (**G**).

Reporter expression (in green) is shown in oligodendroglial lineage cells identified by the nuclear expression of OLIG2 (in blue) and the cytosolic immunoreactivity for CC1 (in red). White arrowheads indicate CC1+ and NDRG1- cells. Scale bar = 50μm. (**H-I**) Quantification of the percentage of OLIG2+ cells that are also NDRG1+ (**H**) or CC1+ (**I**) in the corpus callosum of *TgNdrg1-EGFP* reporter mice at the indicated time points. Percentages were calculated by dividing the number of GFP+ cells by OLIG2+ cells and the average per mouse ± SD is shown. (**J**–**K**) Quantification of the percentage of NDRG1+ cells that are also CC1+ (**J**) or of CC1+ cells that also express NDRG1 (**K**) in the corpus callosum of *TgNdrg1-EGFP* reporter mice at P10, P16 and P21. (**$p < 0.01$ ****$p < 0.0001$, One-way ANOVA, Tukey's post-hoc test)

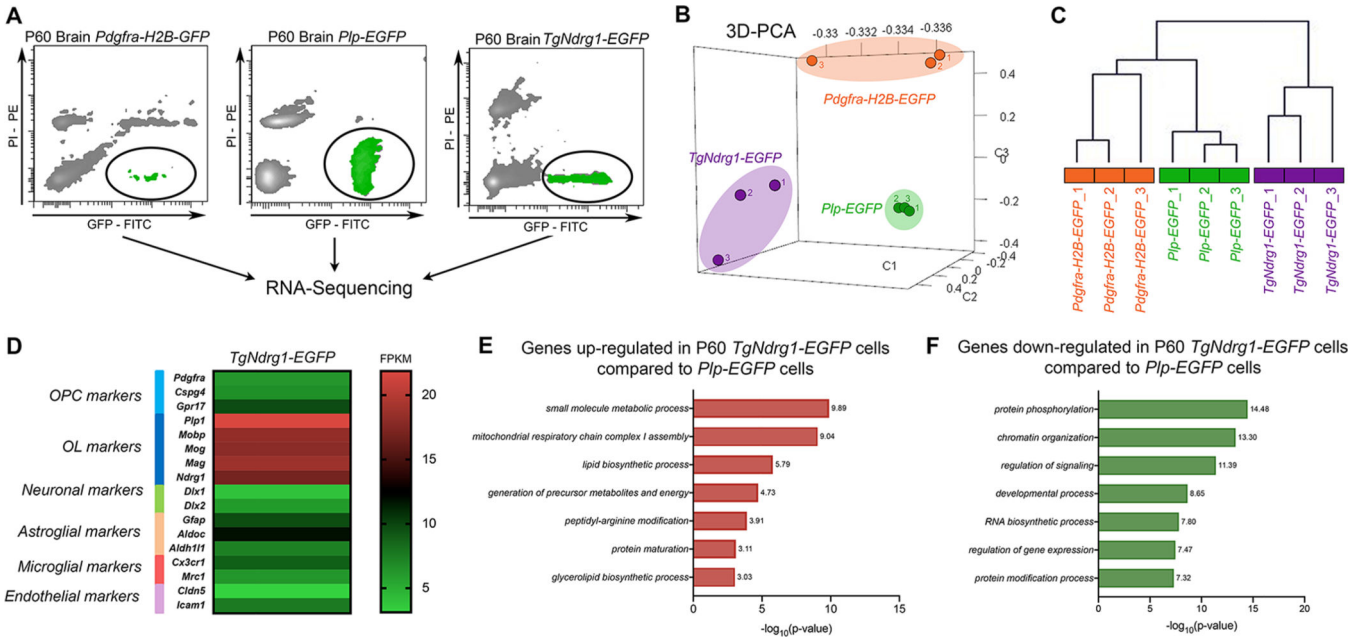

Figure 3. Comparative transcriptomic analysis of NDRG1+ myelinating OLs and PLP+ OLs in the adult brain reveals a unique transcriptional signature.

(**A**) Representative fluorescence-activated cell sorting plots of cells used for RNA-Sequencing. Adult progenitors (OPCs) were sorted from the brains of P60 *Pdgfra-H2B-EGFP* reporter mice, differentiated oligodendrocytes (OLs) from the brains of adult P60 *Plp-EGFP* mice and myelinating oligodendrocytes were sorted from the brains of adult P60 *TgNdrg1-EGFP* mice. (**B**) 3D principal component analysis (3D-PCA) showing the 3 distinct biological replicates (n=3) for each reporter line. See also Table S1 for mapped read counts. (**C**) Hierarchical clustering of all genes (dendrogram): each column represents the gene expression in a single biological replicate sample (Pearson correlation, using Multi-Experiment Viewer). (**D**) Normalized transcript levels (FPKM) for specific OPC, OL, neuronal, astroglial, microglial and endothelial markers for P60 brain *TgNdrg1-EGFP* samples. (**E**) Gene ontology analysis of categories for transcripts up-regulated in adult P60 *TgNdrg1-EGFP*+ cells compared to P60 *Plp-EGFP*+ cells. See also Table S2 for gene list. (**F**) Gene ontology analysis of categories for transcripts up-regulated in adult P60 *TgNdrg1-EGFP*+ cells compared to P60 *Plp-EGFP*+ cells. See also Table S3 for gene list.

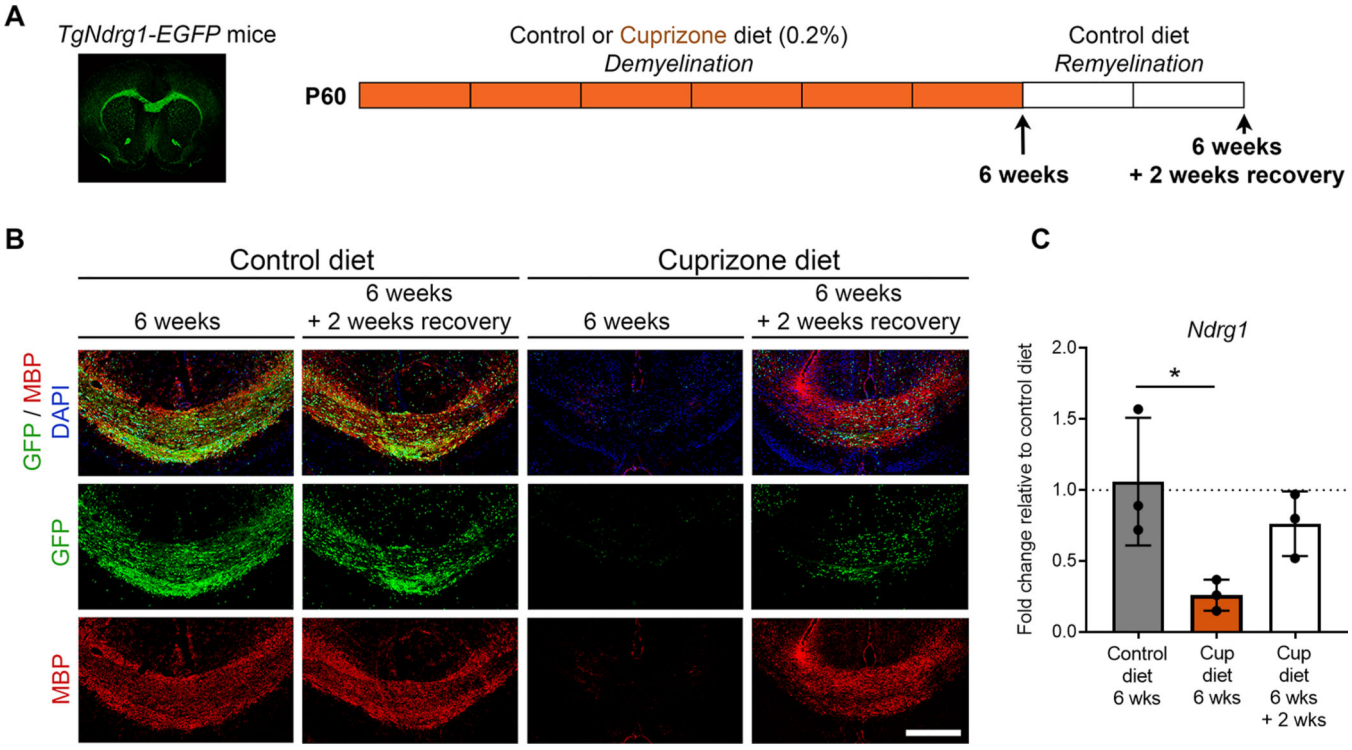

Figure 4. *TgNdrg1-EGFP* reporter line as a tool to study adult demyelination and remyelination

(**A**) Schematics of experimental plan conducted in adult P60 male *TgNdrg1-EGFP* reporter mice fed with control chow diet or cuprizone diet for six weeks, followed, for another cohort, by two weeks of control chow diet. (**B**) Representative confocal image of corpus callosum in coronal brain sections from *TgNdrg1-EGFP* mice fed either chow control diet or 0.2% cuprizone-diet for the indicated time period. Sections were stained with MBP (red) and DAPI (blue). Expression of NDRG1 is in green. Scale bar = 250μm. (**C**) Transcript levels of *Ndrg1* using quantitative real-time PCR analysis. Corpus callosum tissues were isolated after control diet (6 wks), cuprizone-treatment (6 wks) and during the recovery phase (6 wks + 2 wks). Data represent average values normalized to control chow (6 wks) ± SD for n=3 mice (*$p < 0.05$, one-way ANOVA with Dunnett's post-hoc test).

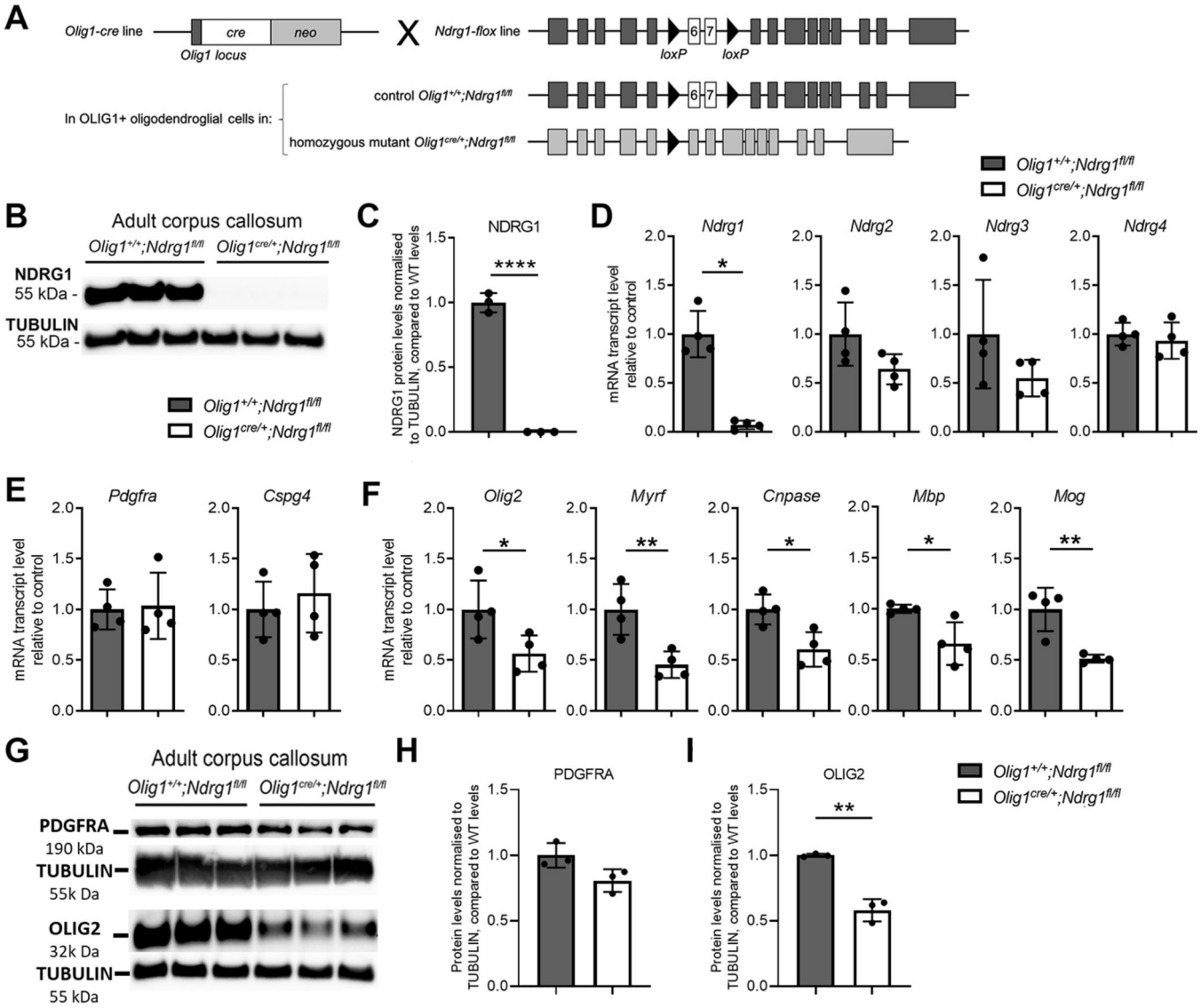

Figure 5. Specific ablation of *Ndrg1* in oligodendroglial lineage affects developmental myelination.

(**A**) Schematic illustrating the conditional knock-out breeding strategy used to generate the *Olig1cre;Ndrg1floxed* line, leading to deletion of *Ndrg1* exons 6 and 7 in oligodendroglial lineage cells. (**B**) Representative western blot of NDRG1 in adult corpus callosum protein lysate from control $Olig1^{+/+};Ndrg1^{fl/fl}$ and mutant $Olig1^{cre/+};Ndrg1^{fl/fl}$ mice. Tubulin was used as loading control. (**C**) Quantification of NDRG1 protein levels normalized to Tubulin- expression; histograms represent average values ± SD for n=3 samples (**** $p < 0.0001$, unpaired t-test). (**D**) Quantitative real-time PCR analysis of *Ndrg1, Ndrg2, Ndrg3* and *Ndrg4* on corpus callosum tissues of adult control $Olig1^{+/+};Ndrg1^{fl/fl}$ and mutant $Olig1^{cre/+};Ndrg1^{fl/fl}$ mice. Data represents average values normalized to control samples ± SD for n=4 mice (* $p < 0.05$, Student's t-test). (**E-F**) Quantitative real-time PCR analysis of progenitors (**E**) and oligodendroglial (**F**) transcripts in corpus callosum samples of adult control $Olig1^{+/+};Ndrg1^{fl/fl}$ and mutant $Olig1^{cre/+};Ndrg1^{fl/fl}$ mice. Data represents average

values normalized to control samples ± SD for n=4 mice (*$p < 0.05$, **$p < 0.01$, Student's t-test). (**G**) Representative western blot of PDGFRA and OLIG2 in adult corpus callosum total lysate from control *Olig1*$^{+/+}$;*Ndrg1*$^{fl/fl}$ and mutant *Olig1*$^{cre/+}$;*Ndrg1*$^{fl/fl}$ mice. Tubulin was used as control. (**H-I**) Quantification of PDGFRA and OLIG2 protein levels. Data were normalized to Tubulin-α expression; histograms represent average values ± SD for n=3 samples.

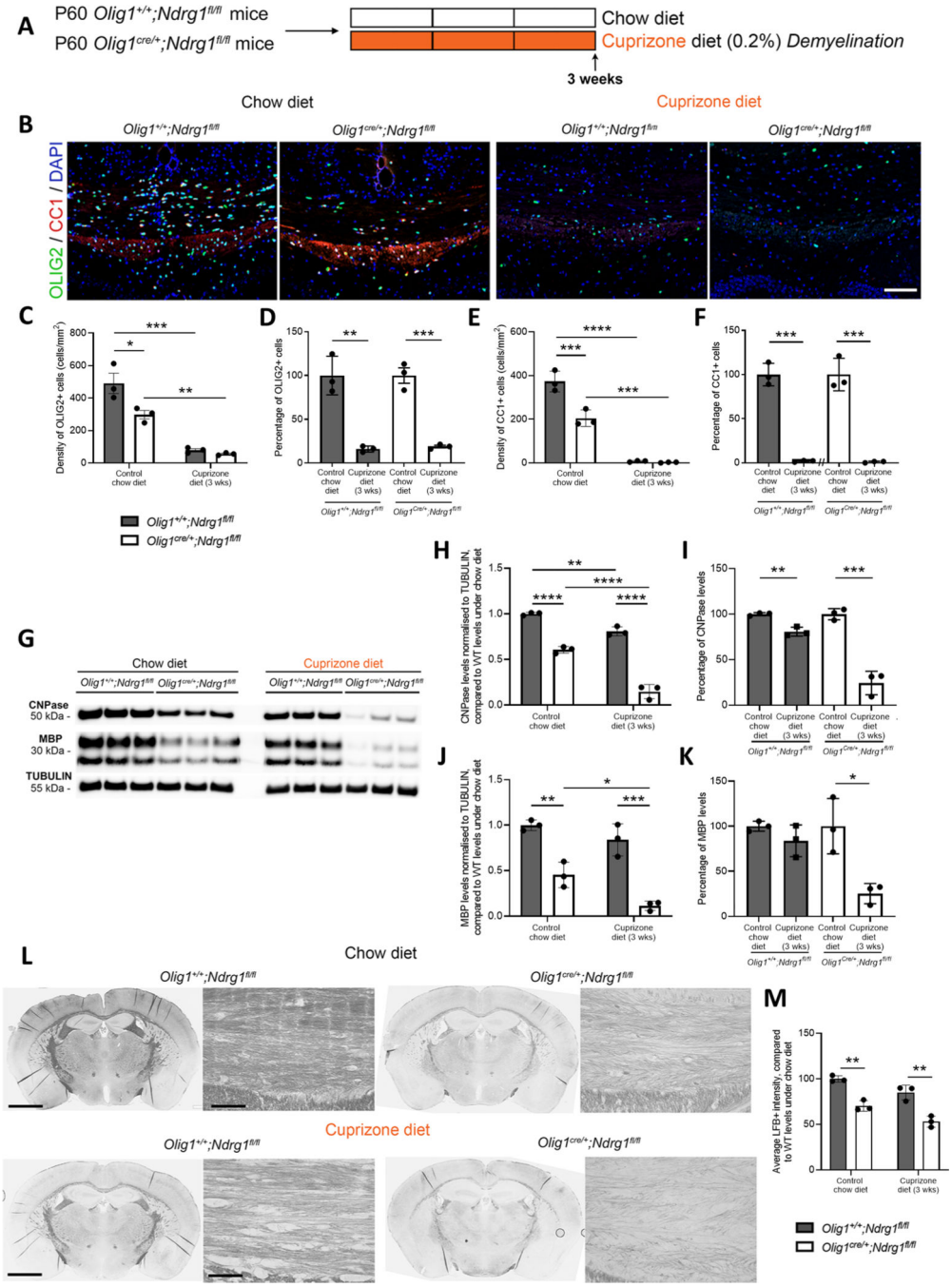

Figure 6. Specific ablation of *Ndrg1* in oligodendroglial lineage cells induces susceptibility to myelin damage.

(**A**) Schematics of experimental plan conducted in adult control *Olig1*$^{+/+}$;*Ndrg1*$^{fl/fl}$ and mutant *Olig1*$^{cre/+}$;*Ndrg1*$^{fl/fl}$ mice, fed with cuprizone diet (n=3) for three weeks. (**B**) Representative confocal image of coronal brain sections from adult control *Olig1*$^{+/+}$;*Ndrg1*$^{fl/fl}$ and mutant *Olig1*$^{cre/+}$;*Ndrg1*$^{fl/fl}$ mice after control chow or cuprizone diet, stained for OLIG2 (green), CC1 (red) and DAPI (blue). Scale bar = 500µm. (**C-E**) Quantification of the density of OLIG2+ cells and CC1+ cells in the corpus callosum

of adult control *Olig1*$^{+/+}$;*Ndrg1*$^{fl/fl}$ and mutant *Olig1*$^{cre/+}$;*Ndrg1*$^{fl/fl}$ mice. Data represents average number of OLIG2+ and CC1+ cells per mm^2 in the corpus callosum area ± SD for n=3 mice (*$p < 0.05$, **$p < 0.01$, ***$p < 0.001$, ****$p < 0.0001$, Two-way ANOVA with Tukey's post-hoc test). (**D-F**) Percentage of OLIG2+ cells and of CC1+ cells in the corpus callosum of adult control *Olig1*$^{+/+}$;*Ndrg1*$^{fl/fl}$ and mutant *Olig1*$^{cre/+}$;*Ndrg1*$^{fl/fl}$ mice compared to their respective genotype under control chow diet. Data represents average percentage of OLIG2+ and CC1+ cells per mm^2 in the corpus callosum area ± SD for n=3 mice (**$p < 0.01$, ***$p < 0.001$, unpaired t-test). (**G**) Representative western blot of CNPase, MBP and TUBULIN in adult corpus callosum total protein lysates from control *Olig1*$^{+/+}$;*Ndrg1*$^{fl/fl}$ and mutant *Olig1*$^{cre/+}$;*Ndrg1*$^{fl/fl}$ mice either on chow or on cuprizone diet for the indicated time period. (**H-J**) Quantification of CNPase and MBP protein levels, normalized to tubulin expression. Data represents average values ± SD for n=3 mice. (*$p < 0.05$, **$p < 0.01$, ***$p < 0.001$ and ***$p < 0.0001$, Two-way ANOVA with Tukey's post-hoc test). (**I-K**) Percentage of CNPase and MBP protein levels in the corpus callosum of adult control *Olig1*$^{+/+}$;*Ndrg1*$^{fl/fl}$ and mutant *Olig1*$^{cre/+}$;*Ndrg1*$^{fl/fl}$ mice compared to their respective genotype under control chow diet. Data represents average percentage of CNPase and MBP levels in the corpus callosum area ± SD for n=3 mice (*$p < 0.05$, **$p < 0.01$, ***$p < 0.001$, unpaired t-test) (**L**) Representative images of coronal brain sections stained with Luxol fast blue from adult control *Olig1*$^{+/+}$;*Ndrg1*$^{fl/fl}$ and mutant *Olig1*$^{cre/+}$;*Ndrg1*$^{fl/fl}$ mice, fed either chow diet or 0.2% cuprizone diet. Scale bars = 2mm on gross image (left) and 50μm on high magnification (right). (**M**) Quantification of Luxol fast blue (LFB) intensity in the corpus callosum (CC) of adult control *Olig1*$^{+/+}$;*Ndrg1*$^{fl/fl}$ and mutant *Olig1*$^{cre/+}$;*Ndrg1*$^{fl/fl}$ mice. Data represents average intensity percentage in corpus callosum regions, normalized to the intensity the control group under chow diet, ± SD for n=3 mice. ((*$p < 0.05$ and **$p < 0.01$, Two-way ANOVA with Tukey's post-hoc test).